OPEN

Period-3 dominant phase synchronisation of *Zelkova serrata*: border-collision bifurcation observed in a plant population

Kenshi Sakai[1*], Yoshinobu Hoshino[2], Awadhesh Prasad[3], Atsuko Sugawara Fukamachi[4] & Akira Ishibashi[4]

The population synchrony of tree seed production has attracted widespread attention in agriculture, forestry and ecosystem management. Oaks usually show synchronisation of irregular or intermittent sequences of acorn production, which is termed 'masting'. Tree crops such as citrus and pistachio show a clear two-year cycle (period-2) termed 'alternate bearing'. We identified period-3 dominant phase synchronisation in a population of *Zelkova serrata*. As 'period-3' is known to provide evidence to imply chaos in nonlinear science, the observed period-3 phase synchronisation of *Zelkova serrata* is an attractive real-world phenomenon that warrants investigation in terms of nonlinear dynamics. Using the Hilbert transform, we proposed a procedure to determine the fractions of periods underlying the survey data and distinguished the on-year (high yield year) and the off-year (low yield year) of the masting. We quantified the effects of pollen coupling, common environmental noise and individual variability on the phase synchronisation and demonstrated how the period-3 synchronisation emerges through a border-collision bifurcation process. In this paper, we propose a model that can describe diverse behaviours of seed production observed in many different tree species by changing its parameters.

The highly synchronised fluctuation of annual seed production is common in perennial plant species. Among such species, acorn masting has particularly attracted interest in many fields of research[1–4]. In silviculture, prediction of masting behaviour in forest stands is necessary for approaches that promote natural regeneration[5,6]. As acorns are a substantial food source for wild animals[2], it is important to understand masting for ecological management[7–10]. 'Alternate bearing' refers to tree crops that produce heavy crops one year (the 'on' year) and light crops the following year (the 'off' year). Citrus (e.g., oranges, lemons and mandarins), pistachios and chestnuts are crops that show pronounced alternate bearing[11–15]. Acorn masting and alternate bearing also have been investigated in terms of the synchronisation of ensembles of trees[16–19]. In nonlinear physics, the synchronisation of ensembles of oscillators is known to be caused by mutual coupling or common identical noise[20,21]. Many types of coupling, such as indirect global and local coupling[16–19] and direct coupling[22], have been investigated. The common noise-induced synchrony[23–27] is known as the Moran effect in population ecology. In a 15-year field survey, we observed period-3 dominant phase synchronisation in a population of 106 individuals of *Zelkova serrata*. To date, the majority of masting behaviour has been recognised as irregular and/or intermittent sequences and alternate bearing of tree crops is generally period-2. Therefore, the period-3 dominant synchronisation identified here is unique. In particular, period-3 is a special term in nonlinear dynamics, as it has been proven that certain dynamics of period-3 can generate any periods including chaos[28]. Thus, elucidation of the mechanism of period-3 phase synchronisation in *Zelkova serrata* will contribute to understanding the variety of periods synchrony reported in many perennial plant species.

[1]Division of Environmental and Agricultural Engineering, Institute of Agriculture, Tokyo University of Agriculture and Technology, Tokyo, 183-8509, Japan. [2]Division of Environment Conservation, Institute of Agriculture, Tokyo University of Agriculture and Technology, Tokyo, 183-8509, Japan. [3]Department of Physics and Astrophysics, University of Delhi, Delhi, 110007, India. [4]Department of Environment Conservation, Graduate School of Agriculture, Tokyo University of Agriculture and Technology, Tokyo, 183-8509, Japan. *email: ken@cc.tuat.ac.jp

The objective of this study was to clarify the mechanism underlying the period-3 dominant synchronisation in the population of *Zelkova serrata* surveyed. We developed a method to quantify various periodic compositions coexisting in an ensemble time series. We demonstrated a globally coupled map of the resource budget model (hereafter GCM-RBM)[16] to model the period-3 dominant phase synchronisation of *Zelkova serrata* as its masting behaviour.

The GCM-RBM has been commonly used to model the population synchrony of cross-pollinated plants[16–18]. At a certain magnitude of coupling strengths (β), the group consisting of N RBMs is strongly synchronised so that its dynamics can be represented by a one-dimensional map. We demonstrate how the period-3 emerges from a tangential bifurcation of the GCM-RBM whose map (characterised as a border-collision bifurcation) is piecewise smooth and piecewise monotonic[29,30]. We also estimated control parameters (R_C and β) of the GCM-RBM for the survey data for *Zelkova serrata*. The proposed approach is expected to be a powerful method to understand the mechanisms of synchronisation in various perennial plant species.

Materials and Methods

Field survey. *Zelkova serrata* is a diclinous monoecious tree distributed in East Asia and flowers in April and May. The leaf colour changes to vivid red in autumn and the leaves on fruiting twigs change colour much earlier than those on non-fruiting twigs (see Supplementary Fig. S1). On the basis of visual inspection from the ground in two weeks of mid-November, the seed production level was classified into 10 classes. This method is popular in vegetation surveys[31,32]. Data from a population of 106 trees acquired over 15 years from 2003 to 2017 were analysed. This primary survey was conducted in the area bounded by longitude 139°28′45.57″E to 139°28′45.84″E and latitude 35°40′11.99″N to 35°40′31.90″N in Fuchu City, Tokyo, Japan. We also conducted a additional survey for 48 trees since 2006 in the area bounded by longitude 139°41′27.64″E to 139°41′40.58″E and latitude 35°41′25.04″N to 35°41′27.30″N in Shinjuku District located 20 km west of Fuchu City.

Fraction of the period-Q sequence. For identification of the 'on-year' and the 'off-year' for a single time series $x(t)$, we defined the flag index $ON(t)$ as a step function by employing phase-based and amplitude-based definitions.

As the phase angle $\theta(t)$ of a single time series $x(t)$ is needed to define $ON(t)$, it is given by

$$\theta(t) = \text{angle}(\text{HT}[X(t) - \overline{X}]) \tag{1}$$

where HT is the Hilbert transform of the true signal, $\overline{X}$ is the time average of $X(t)$[31–38].

We used MATLAB® for this calculation with the signal processing toolbox code 'hilbert'[32,33] for $\{X(t, i); t = 1, \ldots, T, i = 1, \ldots, N\}$ using

$\theta(:, :) = \text{angle}(\text{hilbert}(X(:, :) - \text{mean}(X(:, :), 1)))$.

In the phase-based definition, we used the phase $\frac{\pi}{2}$ as a threshold to distinguish the 'on-year' and the 'off-year'. $|\theta(t)| < \frac{\pi}{2}$ and $|\theta(t)| \geq \frac{\pi}{2}$ correspond to the on-year and the off-year, respectively.

$$ON_P(t) = \begin{cases} 1 & |\theta(t)| < \dfrac{\pi}{2} \\ 0 & |\theta(t)| \geq \dfrac{\pi}{2} \end{cases} \tag{2}$$

In the amplitude-based definition, we used the time average of $x(t)$ as a threshold to distinguish the 'on-year' and the 'off-year'. When $x(t)$ is larger than $\overline{x} = \sum_{t=1}^{T} x(t)$, then year t is considered to be the 'on-year'.

$$ON_A(t) = \begin{cases} 1 & x(t) > \overline{x} \\ 0 & x(t) \leq \overline{x} \end{cases} \tag{3}$$

Matching between $ON_A(t)$ and $ON_P(t)$ was examined with 1600 combinations of the two control parameters (β and R_C) used in Fig. 7 to show that the two indices were identical.

The afore-mentioned two definitions of $ON(t)$ can be expanded to the ensemble $\{x_i(t); t = 1, 2, \ldots, T, i = 1, 2, \ldots, N\}$ to obtain $ON_i(t)$ for each tree i as follows,
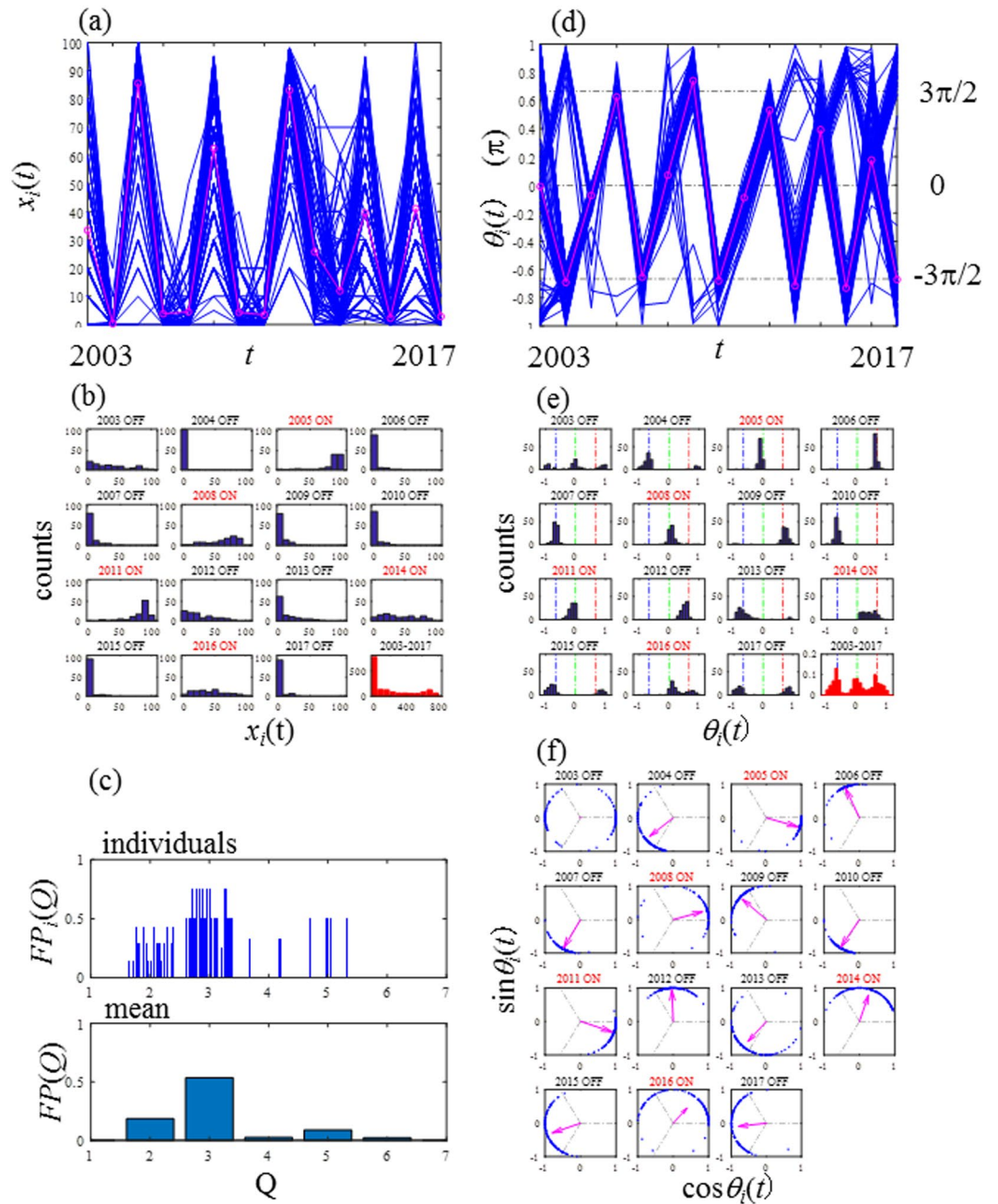
$$ON_{A,i}(t) = \begin{cases} 1 & x_i(t) > \overline{x}_i \\ 0 & x_i(t) \leq \overline{x}_i \end{cases}, \tag{4}$$

where

$$\overline{x}_i = \frac{1}{T} \sum_{t=1}^{T} x_i(t),$$

and

$$ON_{P,i}(t) = \begin{cases} 1 & |\theta_i(t)| < \dfrac{\pi}{2} \\ 0 & |\theta_i(t)| \geq \dfrac{\pi}{2} \end{cases}. \tag{5}$$

Figure 1. Seed production of 106 *Zelkova serrata* trees over 15 years (2003–2016) at Fuchu City, Tokyo, Japan. (**a**) Seed production $x_i(t)$. The mean seed production $X(t)$ (thick solid line in magenta) demonstrates a clear period-3 pattern. (**b**) Histograms of $x_i(t)$. (**c**) Fractions of period-Q for individuals, $FP_i(Q)$, and for the population, $FP(Q)$. (**d**) Phase of the seed production $\theta_i(t)$ with the median of phase $\Theta(t)$ in magenta. (**e**) Histograms of $\theta_i(t)$. (**f**) Circle maps.

To investigate the phase synchronisations of masting in a population of trees, it is important to observe the composition of periods in individual trees and the population. Here, we propose a practical means to determine the composition of periodic components. For instance, period-2 and period-3 sequences are defined as 'ON $\Rightarrow$ OFF $\Rightarrow$ ON' and 'ON $\Rightarrow$ OFF $\Rightarrow$ OFF $\Rightarrow$ ON', respectively. Thus, a period-Q sequence is defined as the sequence where one 'on-year' at year t is followed by $Q - 1$ for 'off-year' and 'on-year' arises at year $t + Q$. The fraction of period-Q in the ith tree's time series is determined by

$$FP_i(Q) = \frac{Q}{(T-1) - \mod(T-1, Q)} \sum_{t=1}^{T-Q} \left[ON_i(t) ON_i(t+Q) \prod_{j=2}^{Q-1} (1 - ON_i(t+j)) \right].$$

(6)

where $ON_i(t)$ is determined by Eqs (4, 5).

The fraction of period-Q representing a population is given by

$$FP(Q) = \text{mean}(FP_i(Q)), \quad i = 1, 2, \ldots, N. \tag{7}$$

The median and mode can be used to represent a population as well as the mean.

Measures of synchrony. Given that we focused on the phase synchronisation, we employed the notion of in-phase and out-of-phase analysis[22]. The fraction of in-phase in a population $\{x_i(t); i = 1, 2, \ldots, N, t = 1, 2, \ldots, T\}$ is also used[22] to measure the phase synchronisation of a population of trees. If the arbitrary pair of $x_i(t)$ and $x_j(t)$ show in-phase behaviour between year t and year $t + 1$, then

Let $x_i(t)$ be the yield of the ith tree in year t, and define $\phi(i, j, t)$ as the phase between the ith and j^{th} tree:

$$\varnothing(i, j, t) = \{x_i(t + 1) - x_i(t)\} \times \{x_j(t + 1) - x_j(t)\}. \tag{8}$$

The fractions of in-phase movements of the ith tree relative to the remaining trees in the population is defined as

$$f_{\text{IN}}^i(t) = \frac{1}{N - 1} \sum_{j=1, j \neq i}^{N} H_{\text{IN}}[\varnothing(i, j, t)]. \tag{9}$$

where H_{IN} is given as Heaviside step function, however, $H_{\text{IN}} = 1$, when $x_i(t + 1) - x_i(t) = x_j(t + 1) - x_j(t) = 0$.

The fraction of in-phase of the population (size N) at time t is expressed by $f_{\text{IN}}(t)$.

F_{IN} denotes the time average of $f_{\text{IN}}(t)$.

Model. The resource budget model (RBM) is described below and has been used previously to model masting and alternate bearing[16,39]. Let $S_i(t)$ be the amount of resource reserves at the beginning of year t for tree i. If the accumulated resource $S_i(t) + P_S$ exceeds the threshold of the pool (L_T), then the excess amount $S_i(t) + P_S - L_T$ is used for flowering C_f^i.

$$S_i(t + 1) = \begin{array}{ll} S_i(t) + P_S, & S_i(t) + P_S \leq L_T \\ S_i(t) + P_S - C_f^i(t) - C_a^i, & S_i(t) + P_S > L_T \end{array}, \tag{10}$$

$$C_f^i = S_i(t) + P_S - L_T \tag{11}$$

The cost of pollinating flowers and bearing fruit is designated by C_a^i. The cost ratio $R_C = C_a^i/C_f^i$ is a constant.

$$C_a^i = R_C C_f^i \tag{12}$$

After the reproductive stage, the accumulated resource becomes $L_T - C_a^i = L_T - R_C C_f^i$.

The RBM is a one-dimensional map modelled by Eqs (10–12), where $-R_C$ is the slope at the fixed point of the RBM. Isagi (1996) introduced the fruiting efficiency of a tree, $Y(t)$[16], as a global coupling term.

$$Y(t) = \left[\frac{1}{(N - 1)P_0} \sum_{j=1, j \neq i}^{N} C_f^i(t) \right]^{\beta} \tag{13}$$

where β is the strength of pollen coupling and N denotes the population size.

Equation (12) is replaced by Eq. (14) to model the pollen coupling:

$$C_a^i = R_C C_f^i Y(t) \tag{14}$$

As described above, the GCM-RBM is established with Eqs (10–14).

To model the phase synchronisation associated with a nontrivial disturbance, we incorporate individual noise (e_I) and common noise (e_C) into the GCM-RBM. Individual noise (e_I) assumes the heterogeneity of trees[24]. Common noise (e_C) can induce synchrony, which is known as the Moran effect[25].

These noise types are imposed on P_S in the following manner:

$$P_S^i(t) = P_0\{1 + e_C\sigma(t)\}\{1 + e_I\delta^i(t)\}. \tag{15}$$

Here, the random number $\sigma(t)$ is drawn from the normal random number $N(\mu, \sigma^2) = (0, 1)$, and $\delta^{ii}(t)$ is assigned to each tree individually. P_0 is the intrinsic annual surplus. The seed production level $x_i(t)$ obtained in the survey (Fig. 1(a)) is considered proportional to $C_s^i = C_f^i Y(t)$ in the GCM-RBM. In the numerical simulations, P_0 and L_T were set as 10 and 100, respectively,
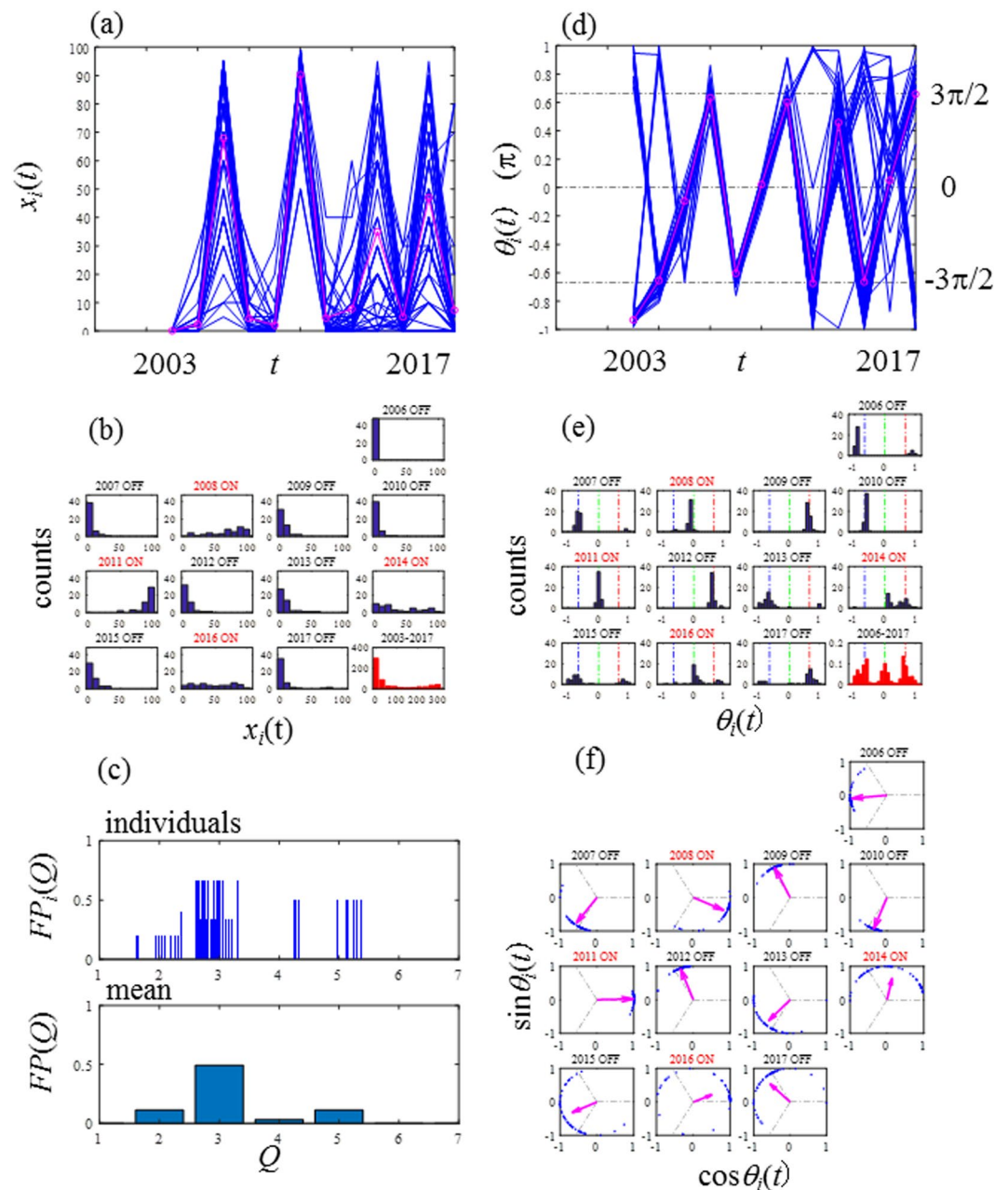
Figure 2. Seed production of 48 *Zelkova serrata* trees over 12 years (2006–2017) at Shinjuku District, Tokyo, Japan. (**a**) Seed production $x_i(t)$. The average production $X(t)$ (thick solid line in magenta) demonstrates a clear period-3 pattern. (**b**) Histograms of $x_i(t)$. (**c**) Fractions of period-Q for individuals; $FP_i(Q)$ and the population; $FP(Q)$. (**d**) Phase of the seed production $\theta_i(t)$ with the median of phase $\Theta(t)$ in magenta. (**e**) Histograms of $\theta_i(t)$. (**f**) Circle maps.

Results and Discussion

Field experiments. Figure 1 shows the results obtained in the primary survey at Fuchu City. The seed production level of the individual trees, $x_i(t)$ and annual (ensemble) mean of the population at year t, $X(t) = \frac{1}{N}\sum_{i=1}^{N} x_i(t)$, are shown in Fig. 1(a). $X(t)$ mostly shows period-3 cycles of an on-year (high-production year) followed by two consecutive off-years (low-production years). Figure 1(b) shows the histograms of seed production level. Here, the on-year of the population was determined by the median of $ON_{P,i}(t)$, $i = 1, 2, …, N$ for $t = 2003, 2005, 2008, 2011, 2014$ and 2016. The histogram for the 15-year total is shown in the last subplot of Fig. 1(b) in red, showing that 70.3% (approximately two-thirds) of the counts are classified in the two lowest classes: 0–10 and 11–20. In Fig. 1(c), the fraction of periods is represented by $FP_i(Q)$ and $FP(Q)$ for each individual tree and the population, respectively. In $FP_i(Q)$ plots, several individual trees showed components of period-4 and/or larger periods; however, it is clearly identified that the period-3 is dominant followed by period-2 for these plots, i.e., $FP(3) = 0.5354$ and $FP(2) = 0.1860$. It is clear that the components of period-4 and larger periods are
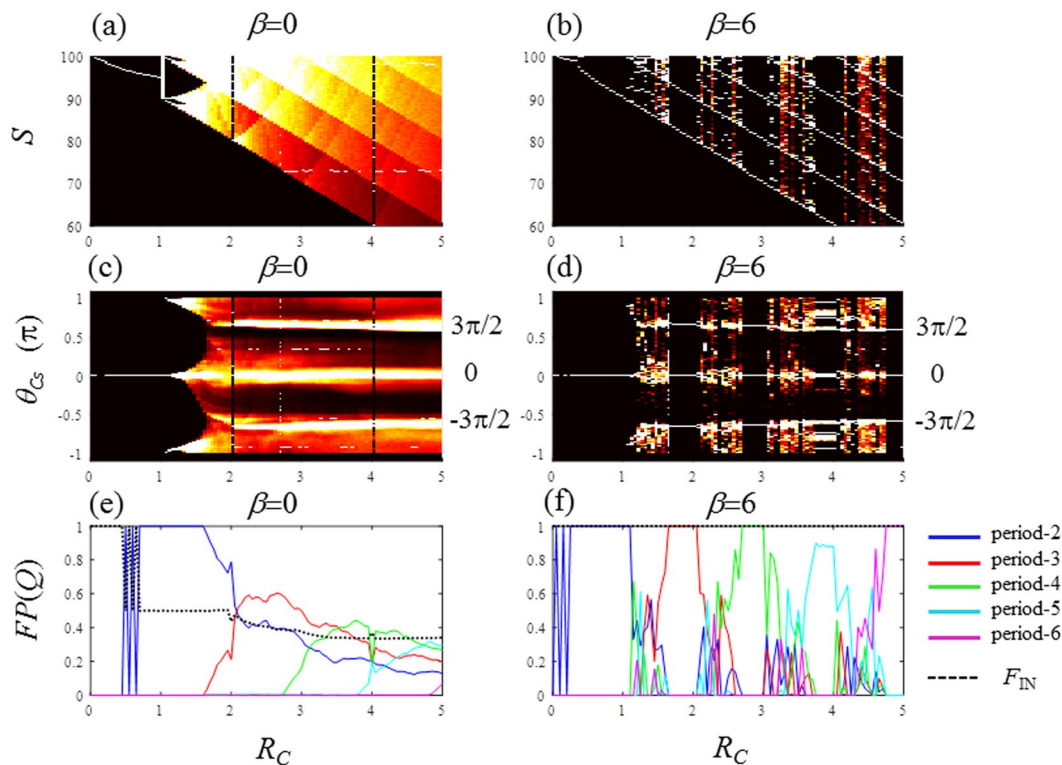
Figure 3. Period-adding bifurcation of the globally coupled map of the resource budget model for the noise-free condition ($e_I = 0$). (**a–d**) Density bifurcation diagrams for S, C_S and θ_{Cs}: (**a**) S: $\beta = 0$, (**b**) S: $\beta = 6$, (**c**) θ_{Cs}: $\beta = 0$, and (**d**) θ_{Cs}: $\beta = 6$. (**e,f**) Fraction of periods $FP(Q)$ for (**e**) $\beta = 0$, and (**f**) $\beta = 6$. $FP(2)$: blue, $FP(3)$: red, $FP(4)$: green, $FP(5)$: cyan, and $FP(6)$: magenta, F_{IN}: dotted line.
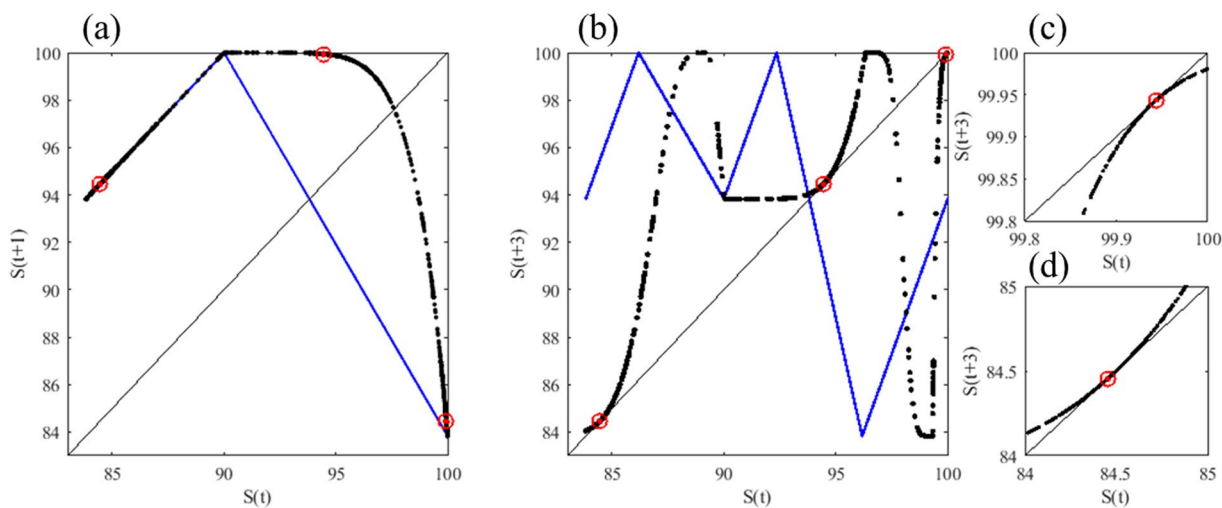
Figure 4. Mechanism generating the period-3 cycle in the tangent bifurcation of the globally coupled map of the resource budget model (GCM-RBM) for $\beta = 0$ (blue thin line) and $\beta = 6$ (black dots). The GCM-RBM is a piecewise smooth and piecewise monotonic map and has border collision period-doubling bifurcations. (**a**) First iterated plots of S, (**b**) third iterated plots of S, (**c**) magnified plots around $S = 99.9438$ and (**d**) magnified plots around $S = 84.4523$.

trivial, e.g., $FP(4) = 0.0252$, $FP(5) = 0.0896$ and $FP(6) = 0.0236$. Thus, $FP(Q)$ defined in Eq. (7) is a powerful tool to quantify the components of periods in an ensemble time-series data set. The phase $\theta_i(t)$ calculated by Eq. (1) for all trees is plotted in Fig. 1(d) and the median of $\{\theta_i(t)\}$ was employed as the representative phase $\Theta(t)$ of the population, which illustrates the period-3 sequence [ON ⇒ OFF ⇒ OFF ⇒ ON] corresponding to [$0 \Rightarrow 2\pi/3 \Rightarrow -2\pi/3 \Rightarrow 0$] consisting of the three fundamental phases (0, $2\pi/3$ and $-2\pi/3$). Figure 1(e) illustrates
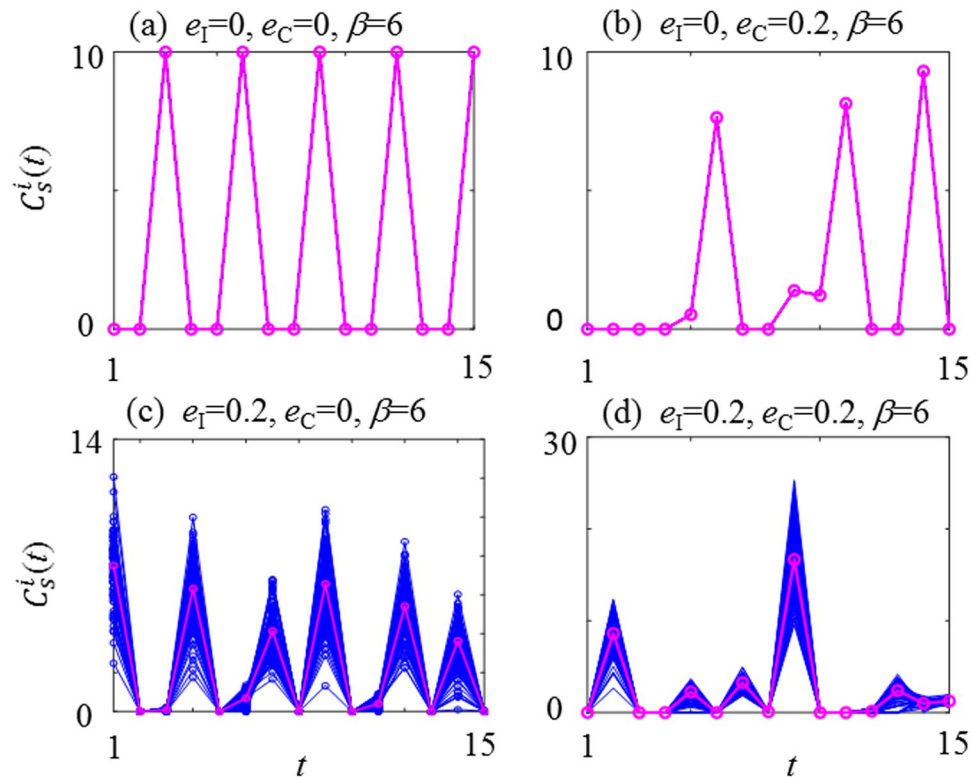
Figure 5. Effects of common noise (e_C) and individual noise (e_I) on seed production (C_S) of *Zelkova serrata*. (**a**) noise free: $e_I = 0$, $e_C = 0$; (**b**) common noise only: $e_I = 0$, $e_C = 0.2$; (**c**) individual noise only: $e_I = 0.2$, $e_C = 0$.; (**d**) common noise and individual noise: $e_I = 0.2$, $e_C = 0.2$, at $R_C = 2$ and $\beta = 6$ for (**a-d**). The average seed productions are plotted in magenta.

the annual changes of the phase histograms and the three fundamental phases are indicated by the three dashed lines. The fundamental phases (0, $2\pi/3$ and $-2\pi/3$), correspond to the on-year (0), the first successive off-year ($2\pi/3$) and the second successive off-year ($-2\pi/3$), respectively. The population of $\theta_i(t)$ is centred at one of the three fundamental phases. The last subplot of Fig. 1(e) in red, which shows the phase histogram for the 15-year term, clearly demonstrates the three evenly distributed peaks corresponding to the three fundamental phases (0, $2\pi/3$ and $-2\pi/3$). Figure 1(f) displays a circle map in each panel in which blue dots are plotted at the points of $(\cos\theta_i(t), \sin\theta_i(t))$. On each panel, the arrow represents the vector (mean$\{\cos\theta_i(t)\}$, mean$\{\sin\theta_i(t)\}$), and the amplitude of the arrow is the order parameter that measures the strength of synchronisation. In the panel for 2003 in Fig. 1(f), the amplitude of the arrow is almost zero. This indicates that desynchronisation occurred in 2003. Therefore, this year should not be an 'on-year' even though $\Theta(2003)$ is almost zero. This is consistent with the median of $\{ON_{P,i}(t), i = 1, 2, \ldots N\}$ indicating an 'off-year' in $t = 2003$. Hence, the phase $\theta(t)$ is useful to diagnose the states of the synchronisation of ensembles of trees. Thus, in Fig. 1, we detected a period-3 dominant phase synchronisation of *Zelkova serrata*. Period-2 synchronisation is common as alternate bearing in crop production, such as that of citrus[39–41] and nuts[42]. In addition, in acorn masting, irregular and/or intermittent sequences are also common[1,43,44]. Therefore, the dominance of the period-3 sequence observed in *Zelkova serrata* is unique and notable. The masting of *Zelkova serrata* is characterised by two key features: (a) two significant periods, i.e., period-3 and period-2 coexist, and (b) the fraction of period-3, *FP*(3), is significantly larger than that of period-2, *FP*(2).

Figure 2 shows the results of the additional survey at Shinjuku District. The key features observed in the primary survey at Fuchu City shown in Fig. 1 are completely consistent with those of the additional survey at Shinjuku District. In particular, the agreements identified in the histograms of seed production (Figs 1(b) vs 2(b)) and the histograms of phase (Figs 1(b) vs 2(b)) are remarkable. The results indicate the presence of a long-range spatial synchronisation between the two populations at Fuchu City and Shinjuku District. The ON–OFF sequence of the two populations was perfectly matched from 2006 to 2017. The presence of such strong spatial synchronisation suggests that global pollen coupling occurred in the range of at least 20 km. The long-ranged spatial synchronisation of masting also has attracted widespread interest[45].

Mechanism of period-3. Figure 3 plots the density bifurcation diagrams of S and θ_{Cs} for three β values. For $\beta = 0$, in Fig. 3(a), the first bifurcation occurs at $R_C = 1$, and at the even integer values of R_C, such as 2, 4, …, periodic solutions appear for S. For $\beta = 6$, in Fig. 3(b), the bifurcation diagrams of S display period-($Q+1$) windows in the interval where $R_C = Q$ belongs[17]. The period of the periodic window increases as R_C increases. This bifurcation is
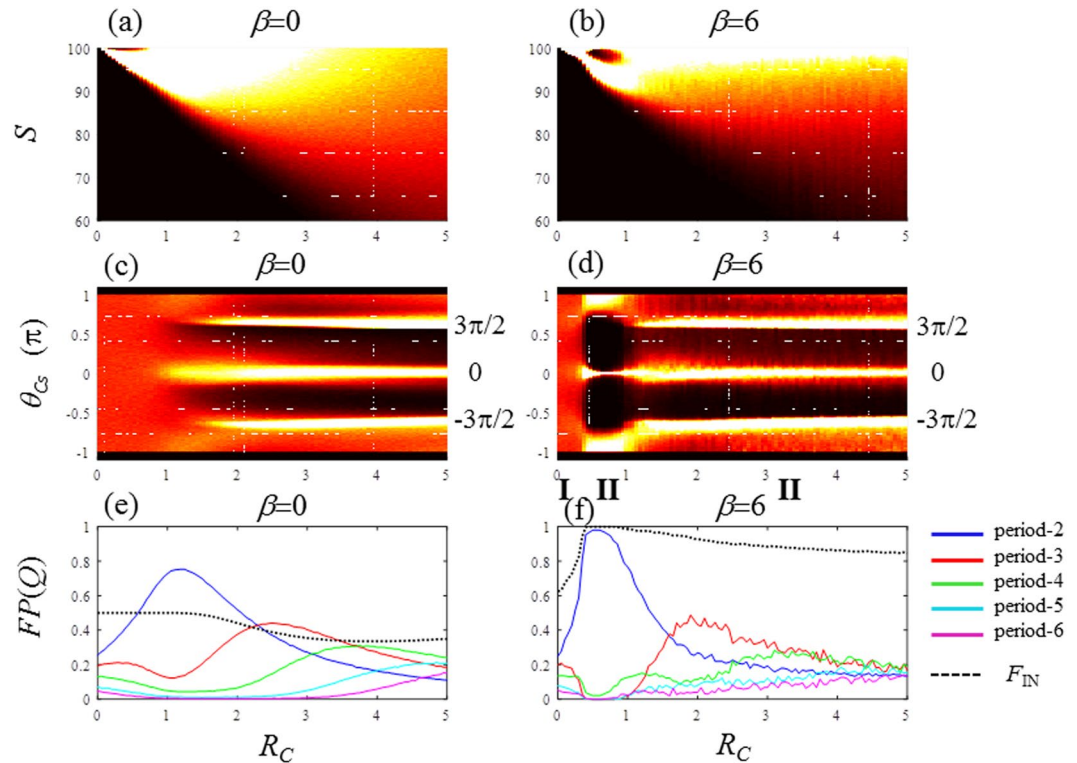
Figure 6. Period-adding bifurcation of the globally coupled map of the resource budget model for the noise-imposed condition ($e_I = 0.2$). (**a–d**) Density bifurcation diagrams for S, and θ_{Cs}: (**a**) S: $\beta = 0$, (**b**) S: $\beta = 6$, (**c**) θ_{Cs}: $\beta = 0$, and (**d**) θ_{Cs}: $\beta = 6$. (**e,f**) Fraction of periods $FP(Q)$ for: (**e**) $\beta = 0$, and (**f**) $\beta = 6$. $FP(2)$: blue, $FP(3)$: red, $FP(4)$: green, $FP(5)$: cyan and $FP(6)$: magenta, F_{IN}: dotted line.

known as the period-adding bifurcation, which is a typical property of border-collision bifurcation explained in Fig. 4[46,47]. The period-adding sequence is clearly demonstrated in Fig. 3(b,f). The density bifurcation diagrams of θ_{Cs} are also displayed in Fig. 3(c,d) for $\beta = 0$ and 6, respectively. It is difficult to measure S for a real tree but it is possible to measure C_S. Therefore, the phase (θ_{Cs}) is a powerful variable to investigate the periods of real-world masting data. The fractions of period-Q {$FP(Q)$; $Q = 2 \ldots, 6$} defined by Eq. (7) are expressed in Fig. 3(e,f) for $\beta = 0$ and 6, respectively. With pollen coupling of $\beta = 6$, $FP(Q)$ is dominant (mostly 1.0) in the interval of the period-Q window, as shown in Fig. 3(f). This result indicates that the perfect period-($R_C + 1$) phase synchronisation arises in the ranges including every digit number of R_C[17]. In the ranges between adjoining period-windows, we can determine the composition of various period-Q ($Q = 2, 3 \ldots$) with $FP(Q)$. The strength of phase synchronisation is estimated as F_{IN}. For example, in Fig. 3(e), at up F_{IN} is 0.5 or smaller because, there is no-coupling as $\beta = 0$. Contrarily, for $\beta = 6$, F_{IN} is maintained at 1 for the entire range of R_C shown in Fig. 3(f), which indicates perfect phase synchronisation.

For $\beta = 6$, a clear period-3 window is present in the range $1.6172 \leq R_C \leq 2.0$ (Fig. 3(b)). Therefore, we selected $R_C = 1.6171$ to generate Fig. 4. The first iterated map is plotted in Fig. 4(a) with thick black dots for $\beta = 6$. The first iterated map for $\beta = 0$ is drawn in a thin blue line, which is a tent map as formulated by Eq. (10). The two first iterated maps of Fig. 4(a) are identical only in $S(t) < L_T$. At the border, $S(t) = L_T$, the left derivative is 1 for both $\beta = 0$ and 6. The right derivatives are $-R_C$ and 0 for $\beta = 0$ and 6, respectively. The third iterated maps for $\beta = 0$ and 6 are plotted in Fig. 4(b). The map for $\beta = 6$ exhibits a clear tangent bifurcation with the three tangency points of 84.4523, 94.4532 and 99.9438. These three tangency points are expressed with three circle marks. Figure 4(c,d) magnify the ranges where the two tangency points of 99.9438 and 84.4523 locate, respectively. The period-3 window of the GCM-RBM is explained by a tangent bifurcation[48,49]. Given that the map ($\beta = 6$) illustrated in Fig. 4(a) is a piecewise smooth and piecewise monotonic map, the bifurcation is the border-collision bifurcation causing the period-adding bifurcation[29,30] as observed in Fig. 3(b,f). This border-collision bifurcation has been studied in the dynamics of switching circuits[29,30]. The existence of the identically same dynamics in electronic circuits and perennial plants implies the universality of the boundary-collision bifurcation in nature.

Effects of noise on the GCM-RBM. The effect of the two types of noise (e_C) and (e_I) on the GCM-RBM was evaluated with four combinations of e_C and e_I at $R_C = 2$ and $\beta = 6$ in Fig. 5(a–d). In the noise-free condition (Fig. 5(a)), perfect period-3 phase synchronisation is apparent. In the case of only common noise, $e_C = 0.2$ (Fig. 5(b)), perfect phase synchronisation is maintained, but four or more consecutive off-year sequences (i.e., larger periodic, irregular and/or intermittent) appear. It should be noted that imposition of common noise (e_C) does not generate any individual disturbances.
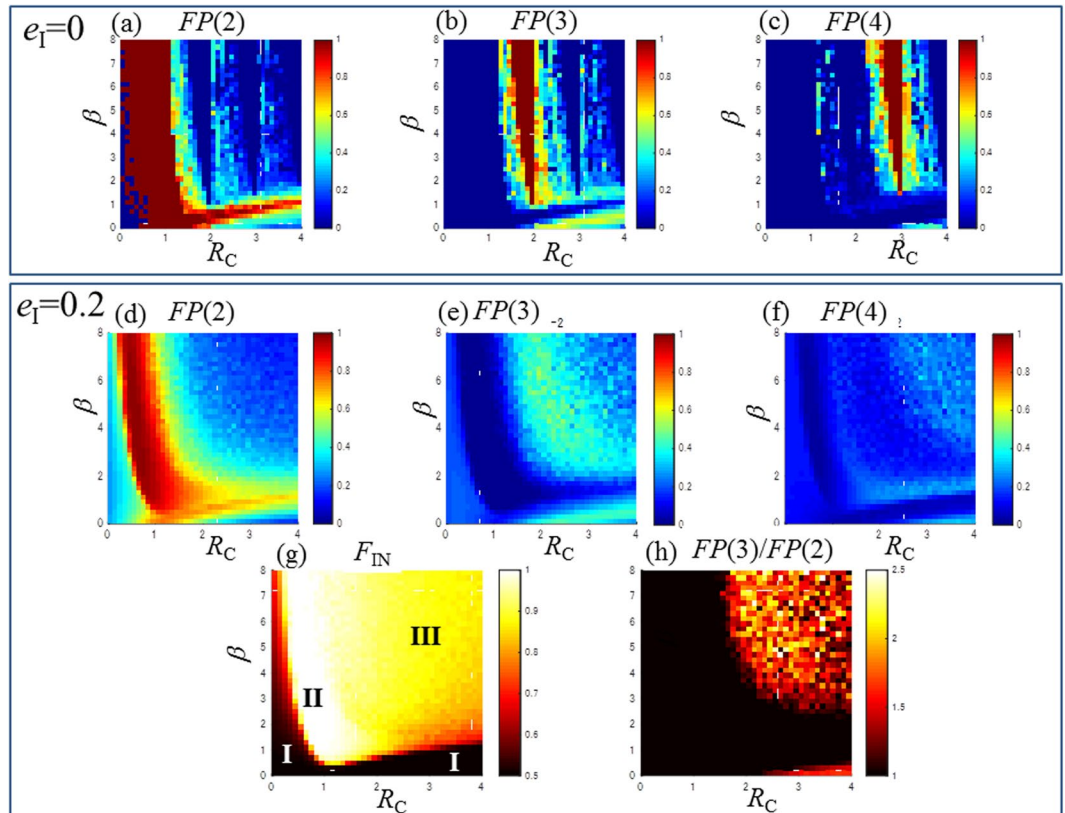
Figure 7. Estimation of the control parameters (R_C and β) of the globally coupled map of the resource budget model for *Zelkova serrata*. (**a**) Fraction of period-2 *FP(2)* for $e_I = 0$, (**b**) fraction of period-3 *FP(3)* for $e_I = 0$, (**c**) fraction of period-4 *FP(4)* for $e_I = 0$, (**d**) fraction of period-2 *FP(2)* for $e_I = 0.2$, (**e**) fraction of period-3 *FP(3)* for $e_I = 0.2$, (**f**) fraction of period-4 *FP(4)* for $e_I = 0.2$, (**g**) fraction of in-phase F_{IN} for $e_I = 0.2$ and (**h**) *FP(3)/FP(2)* ratio for $e_I = 0.2$.

Figure 5(c) shows the case where only individual noise e_I is imposed. The period-3 sequences are clearly identified with some disturbance as observed in Figs 1(a), 2(a). Figure 5(d) demonstrates significant disturbances; however, the appearance of four or more consecutive off-year sequences is inconsistent with the key features of the survey data for *Zelkova serrata*. It is obvious that the individual variability e_I is essential, and the common noise e_C is unnecessary, to explain the period-3 dominant synchronisation of *Zelkova serrata*. Conversely, irregular, intermittent sequences and/or long consecutive off-years have been reported in many other tree species, such as spruce, beech and oak[50]. These reported features correspond to the common noise-imposed case exhibited in Fig. 5(d). Thus, the imposition of both e_I and e_C could account for various masting behaviours[51,52].

In Fig. 6, the density bifurcation diagrams with individual noise $e_I = 0.2$ are plotted in the same arrangements as in Fig. 3. It is difficult to obtain clear structural information from S in Fig. 6(a,b) because of noise presence ($e_I = 0.2$). However, even with noise, the density bifurcation diagrams of θ_{C_s} show clear structural information (Fig. 6(c,d)) indicating the presence of three fundamental phases in the wide range of R_C. By varying R_C, three states are observed in Fig. 6(d,f). In state I, the majority of RBMs behave randomly such that F_{IN} is much smaller than 1.0. In state II, F_{IN} attains 1.0 and the period-2 cycle dominates. In state III, period-3 and larger periods emerge, and the fraction of period-2 *FP(2)* gradually declines. The densities around the three fundamental phases are significantly high in state III as shown in Fig. 6(d).

Parameter studies: estimation of β and R_C for the field data.   To estimate the range of R_C and β for the survey data for *Zelkova serrata*, we conducted a parameter study and present the results in the β–R_C diagrams of Fig. 7. First, we show the noise-free conditions in Fig. 7(a–c) corresponding to the fractions of period-2 *FP(2)*, period-3 *FP(3)* and period-4 *FP(4)*, respectively. The region of *FP(2)* = 1 is sickle-shaped, and those of *FP(3)* = 1 and *FP(4)* = 1 are wedge shaped.

For a noise-imposed condition ($e_I = 0.2$), *FP(2)*, *FP(3)* and *FP(4)* are plotted in Fig.7(d–f), respectively. F_{IN} and *FP(3)/FP(2)* are shown in Fig. 7(g,h). The values *FP(3)* = 0.5354 and *FP(3)/FP(2)* = 2.879 were calculated for the primary survey data in Fig. 1. In Fig. 7(e), the range of *FP(3)* = 0.5354 is located above the sickle-shaped region. *FP(3)/FP(2)* = 2.879 also appears in the sickle-shaped region (Fig. 7(h)) and indicates the coexistence of period-3 and period-2 to the same extent as in Fig. 1. The strength of synchronisation is quantified by F_{IN}. F_{IN} is 1 in state II. The β–R_C diagram of F_{IN} is divided into three regions corresponding to the states I, II and III (Fig. 7(g)). State I is the desynchronised region. In state II, *FP(2)* and F_{IN} are near or equal to 1.0, thus indicating almost perfect

9
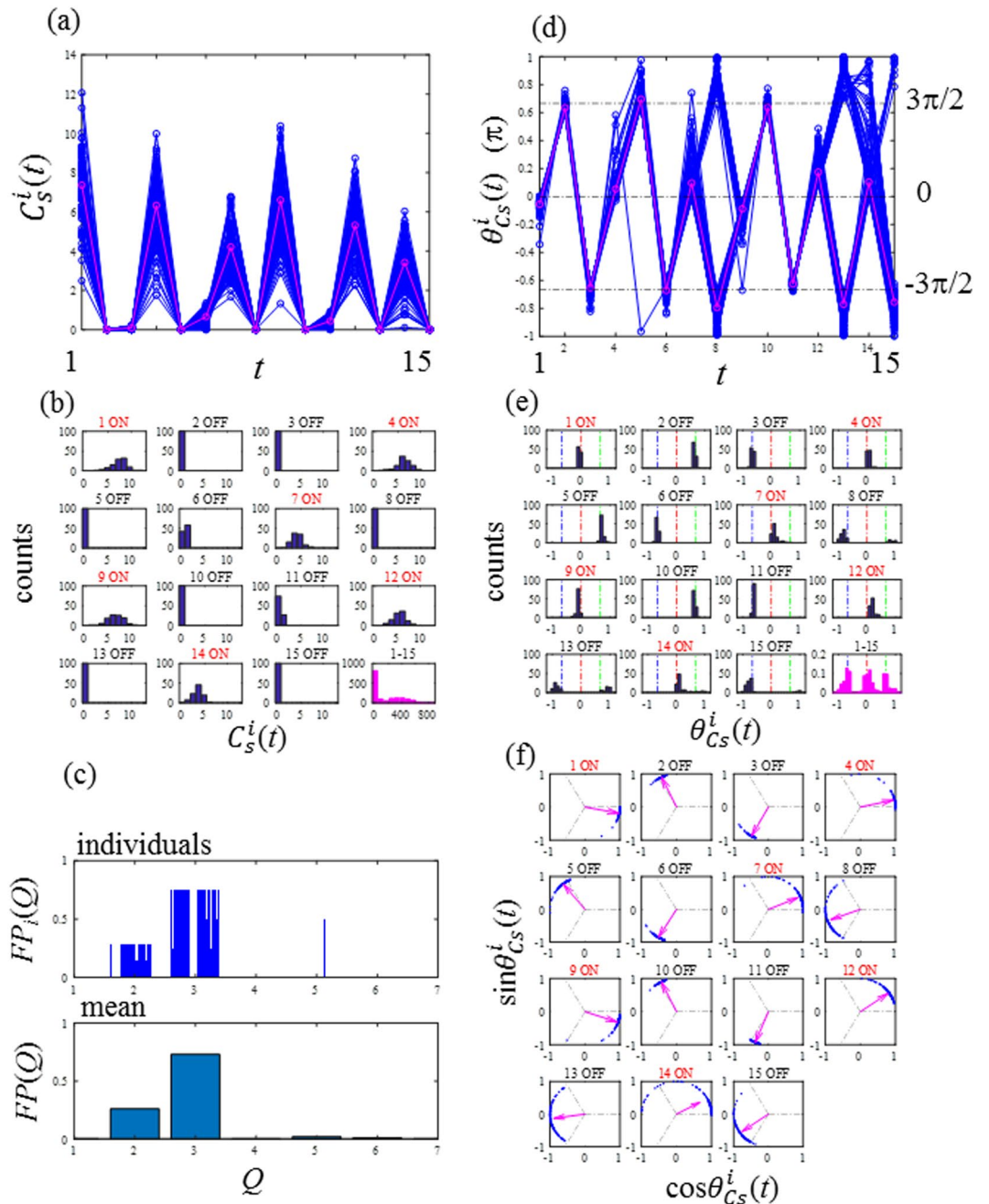
Figure 8. Period-3 phase synchronisation simulated by the globally coupled map of the resource budget model for $R_C = 2$, $\beta = 6$, $e_I = 0.2$ and $e_C = 0$. (**a**) Seed production level C_s^i. The average production (thick solid line) demonstrates a clear period-3 pattern. (**b**) Histograms of C_s^i. (**c**) Fractions of period-Q for individuals, $FP_i(Q)$, and the population, $FP(Q)$. (**d**) Phase of the seed production $\theta_{iCs}(t)$. (**e**) Histograms of $\theta_{iC_s}(t)$. (**f**) Circle maps.

period-2 synchronisation. State III has phase synchronisation consisting of several different periods. The perfect period-$(R_C + 1)$ synchronisation is apparent in every digit number of R_C[17] owing to the period-adding nature of border-collision bifurcation. With increasing noise level e_I, the perfect phase synchronisation moves into imperfect phase synchronisations accompanied with partial desynchronisation. Some fractions of period-$(R_C + 1)$ are still located in the region around the digit numbers of R_C and coexist with other periods. For example, the relatively higher intensity region of $FP(2)$, $FP(3)$ and $FP(4)$ locates around $R_C = 1$, 2 and 3, as shown in Fig. 7(d–f), respectively. As discussed above, we estimated that $R_C = 2$, $\beta = 6$ are $e_I = 0.2$ are appropriate values for *Zelkova serrata*.

Figure 8 shows the results of a numerical experiment of the GCM-RBM with $R_C = 2$, $\beta = 6$, $e_I = 0.2$ and $e_C = 0$. The first key feature of period-3 synchronisation, which is an on-year followed by two consecutive off-years, is clearly demonstrated as most of the seed production (C_S) behaves as a period-3 sequence (Fig. 8(a)). In Fig. 8(b), 70% of the counts were in the two lowest classes in the last panel. Fraction of periods, $FP_i(Q)$ and $FP(Q)$, were

demonstrated in Fig. 8(c) for individual trees and the population, respectively. The $FP(Q)$ is determined as $FP(2) = 0.260$, $FP(3) = 0.730$, $FP(4) = 0.020$, $FP(5) = 0.010$ and $FP(6) = 0.000$. Period-3 is dominant followed by period-2 as $FP(3)/FP(2) = 2.879$, and the other periods are trivial. Three fundamental phases (0, $2\pi/3$, and $-2\pi/3$) are repeated (Fig. 8(d,e)). In the last subplots of Fig. 8(e), the phase θ_{iCs} is evenly located around the three fundamental phases. Importantly, the results presented in Fig. 8 are consistent with those of Figs 1 and 2.

Concluding remarks. Synchronisation of seed production is ubiquitous in many tree species. In this paper, we clarified the mechanism underlying the period-3 dominant synchronisation in populations of *Zelkova serrata* surveyed in Tokyo. We developed a method to determine various periodic compositions coexisting in an ensemble time series. With this method, we found that the phase synchronisations of the populations of *Zelkova serrata* in Fuchu City and Shinjuku District are identical. The observed long-range spatial synchronisation implies global pollen coupling occurred in the range of at least 20 km.

We employed the GCM-RBM to describe the synchrony of the masting of *Zelkova serrata*. When the coupling of the GCM-RBM is sufficiently strong, the dynamics of the GCM-RBM become a piecewise smooth and piecewise monotonic map that is characterised by border-collision bifurcation and the period-adding bifurcation. The mechanism generating period-3 is explained as the tangential bifurcation of the GCM-RBM. The GCM-RBM realised the period-3 dominant phase synchronisation and the key features of the survey data.

The presence of a period-3 solution implies the coexistence of various periodic solutions and chaos in the system. In addition, the GCM-RBM generates periodic solutions larger than period-2 because of its period-adding bifurcation mechanism. Thus, the developed GCM-RBM shows the potential to describe diverse seed-production behaviours observed in many tree species by manipulating its control parameters (R_C and β) and the levels of individual and common noise imposed (e_I and e_C).

References

1. Kelly, D. & Sork, V. L. Mast seeding in perennial plants: why, how, where? *Annual Review of Ecology, Evolution, and Systematics* **33**, 427–447 (2002).
2. Koenig, W. D. & Knopes, J. M. H. The mystery of masting in trees. *American Scientist* **93**, 340–347 (2005).
3. Koenig, W. D., Knopes, M. H., Carmen, W. J. & Pearse, I. S. What drives masting? The phenological synchrony hypothesis. *Ecology* **96**, 184–192 (2015).
4. Pérez-Ramos, I. M., Ourcival, J. M., Limousin, J. M. & Rambal, S. Mast seeding under increasing drought: results from a long-term data set and from a rainfall exclusion experiment. *Ecology* **91**, 3057–3068 (2010).
5. Gärtner, S., Lieffers, V. J. & Macdonald, S. E. Ecology and management of natural regeneration of white spruce in the boreal forest. *Environmental Reviews* **19**, 461–478 (2011).
6. Suzuki, W., Osumi, K. & Masaki, T. Mast seeding and its spatial scale in *Fagus crenata* in northern Japan. *Forest Ecology and Management* **205**, 105–116 (2005).
7. Kon, H., Noda, T., Terazawa, K., Koyama, H. & Yasaka, M. Evolutionary advantages of mast seeding in *Fagus crenata*. *Journal of Ecology* **93**, 1148–1155 (2005).
8. Bieber, C. & Ruf, T. Population dynamics in wild boar *Sus scrofa*: ecology, elasticity of growth rate and implications for the management of pulsed resource consumers. *Journal of Applied Ecology* **42**, 1203–1213 (2005).
9. Pedersen, A. B. & Greives, T. J. The interaction of parasites and resources cause crashes in a wild mouse population. *Journal of Animal Ecology* **77**, 370–377 (2008).
10. Oka, T. *et al.* Relationship Between Changes in Beechnut Production and Asiatic Black Bears in Northern Japan. *Journal of Wildlife Management* **68**, 979–986 (2004).
11. Brown, P. H., Weinbaum, S. A. & Picchioni, G. A. Alternate bearing influences annual nutrient consumption and the total nutrient content of mature pistachio trees. *Trees* **9**, 158–164 (1995).
12. Monselise, S. P. & Goldschmidt, E. E. Alternate bearing in fruit trees. *Horticultural reviews* **4**, 128–173 (2011).
13. Goldschmidt, E. E. The evolution of fruit tree productivity. *Economic Botany* **67**, 51–62 (2013).
14. Meland, M. Effects of different crop loads and thinning times on yield, fruit quality, and return bloom in *Malus × domestica* Borkh. 'Elstar'. *The Journal of Horticultural Science and Biotechnology* **84**, 117–121 (2009).
15. Shalom, L. *et al.* Alternate Bearing in Citrus: Changes in the Expression of Flowering Control Genes and in Global Gene Expression in ON- versus OFF-Crop Trees. *PLOS ONE* **7**, e46930 (2012).
16. Isagi, Y., Sugimura, K., Sumida, A. & Ito, H. How does masting happen and synchronize? *Journal of Theoretical Biology* **187**, 231–239 (1997).
17. Satake, A. & Iwasa, Y. Pollen coupling of forest trees: forming synchronized and periodic reproduction out of chaos. *Journal of Theoretical Biology* **203**, 63–84 (2000).
18. Satake, A. & Iwasa, Y. Spatially limited pollen exchange and a long-range synchronization of trees. *Ecology* **83**, 993–1005 (2002).
19. Akita, K., Sakai, K., Iwabuchi, Y., Hoshino, Y. & Ye, X. Spatial autocorrelation in masting phenomena of *Quercus serrata* detected by multi-spectral imaging. *Ecological Modelling* **215**, 217–224 (2008).
20. Atay, F. M., Jost., J. & Wende, A. Delays, Connection Topology, and Synchronization of Coupled Chaotic Maps. *Physical Review Letters* **92**, 144101 (2004).
21. Kaneko, K. Clustering, coding, switching, hierarchical ordering, and control in a network of chaotic elements. *Physica D* **41**, 137–172 (1990).
22. Prasad, A., Sakai, K. & Hoshino, Y. Direct coupling: a possible strategy to control fruit production in alternate bearing. *Scientific Reports* **7**, 39890 (2017).
23. Satake, A. & Iwasa, Y. The synchronized and intermittent reproduction of forest trees is mediated by the Moran effect, only in association with pollen coupling. *Journal of Ecology* **90**, 830–838 (2002).
24. Lyles, D., Rosenstock, T. S., Hasting, A. & Brown, P. H. The role of large environmental noise in masting: general model and example from pistachio trees. *Journal of Theoretical Biology* **259**, 701–713 (2009).
25. Moran, P. A. P. The statistical analysis of the Canadian lynx cycle. II. Synchronization and meteorology. *Australian Journal of Zoology* **1**, 291–298 (1953).
26. Sviridova, N. & Sakai, K. Noise Induced Synchronization on Collective Dynamics of Citrus Production. *Journal of Japanese Society of Agricultural Machinery and Food Engineers* **78**, 221–226 (2016).

27. Satake, A. & Iwasa, Y. The synchronization and intermittent reproduction of forest trees is mediated by the Moran effect, only in association with pollen coupling. *Journal of Ecology* **90**, 830–838 (2002).
28. Li, T.-Y. & Yorke, J. A. Period Three Implies Chaos. *The American Mathematical Monthly* **82**, 985–992 (1975).
29. Banerjee, S., Karthik, M. S., Yuan, G. & Yorke, J. A. Bifurcations in One-Dimensional Piecewise Smooth Maps-Theory and Applications in Switching Circuits. *IEEE Transactions on Circuits and Systems I: Fundamental Theory and Applications* **47**, 389–394 (2000).
30. Banerjee, S., Ranjan, P. & Grebogi, C. Bifurcations in Two-Dimensional Piecewise Smooth Maps-Theory and Applications in Switching Circuits. *IEEE Transactions on Circuits and Systems I: Fundamental Theory and Applications* **47**, 633–643 (2000).
31. Londo, G. The decimal scale for releves of permanent quadrats. *Vegetatio* **33**, 61–64 (1976).
32. Abe, T. *et al*. Parameterisation and validation of a resource budget model for masting using spatiotemporal flowering data of individual trees. *Ecology Letters* **19**(9), 1129–39 (2016).
33. Selesnick, I. W. The Design of Approximate Hilbert Transform Pairs of Wavelet Bases. *IEEE Transactions of Signal Processing* **50**, 1144–1152 (2002).
34. Blasius, B. & Stone, L. Chaos and Phase Synchronization in Ecological Systems. *International Journal of Bifurcation and Chaos* **10**, 2361 (2000).
35. Feldman, M. Hilbert transform in vibration analysis. *Mechanical Systems and Signal Processing* **25**, 735–802 (2011).
36. Gupta, K., Prasad, A. & Singh, H. P. Analytical signal analysis of strange nonchaotic dynamics. *Physical Review E* **77**, 046220 (2008).
37. Andrade, M. A., Messina, A. R., Rivera, C. A. & Olguin, D. Identification of Instantaneous Attributes of Torsional Shaft Signals Using the Hilbert Transform. *IEEE Transactions of Power Systems* **19**, 1422–1429 (2004).
38. Cazelles, B. & Stone, L. Detection of imperfect population synchrony in an uncertain world. *Journal of Animal Ecology* **72**, 953–968 (2003).
39. Sakai, K. *Nonlinear dynamics and chaos in agriculture systems*. (Elsevier Science, Amsterdam, 2001).
40. Sakai, K., Noguchi, Y. & Asada, S. Detecting Chaos in Citrus Orchard. *Chaos, Solitons & Fractals* **38**, 1274–1282 (2007).
41. Sakai, K. & Noguchi, Y. Controlling chaos (OGY) implemented on a reconstructed ecological two-dimensional map OGY. *Chaos, Solitons & Fractals* **41**, 630–641 (2009).
42. Rosenstock, T. S., Hastings, A., Koenig, W. D., Lyles, D. J. & Brown, P. H. Testing Moran's theorem in an agroecosystem. *Oikos* **120**, 1434–1440 (2011).
43. Masaki, T., Oka, T., Osumi, K. & Suzuki, W. Geographical variation in climatic cue for mast seeding of *Fagus crenata*. *Population Ecology* **50**, 357–366 (2008).
44. Hoch, G., Siegwolf, R. T., Keel, S. G., Körner, C. & Han, Q. Fruit production in three masting tree species does not rely on stored carbon reserves. *Oecologia* **171**, 653–62 (2013).
45. Ishibashi, A. & Sakai, K. Dispersal of allergenic pollen from Cryptomeria japonica and Chamaecyparis obtusa: characteristic annual fluctuation patterns caused by intermittent phase synchronisations. *Scientific Reports* **9**, 11479 (2019).
46. Rollins, E. W. & Hunt, E. R. Exactly solvable model of a physical system exhibiting universal chaotic behaviour. *Physical Review Letters* **49**, 1295–1298 (1982).
47. Buskirk, R. V. & Jeffries, C. Observation of chaotic dynamics of coupled nonlinear oscillators. *Physical Review A* **31**, 3332 (1985).
48. Grebogi, C., Ott, E. & Yorke, J. A. Chaotic Attractors in Crisis. *Physical Review Letters* **48**, 1507–1510 (1982).
49. May, R. Simple mathematical models with very complicated dynamics. *Nature* **261**, 459–467 (1976).
50. Mencuccini, M., Piussi, P. & Zamzi Sulli, A. Thirty years of seed production in a subalpine Norway spruce forest: Patterns of temporal and spatial variation. *Forest Ecology and Management* **76**, 109–125 (1995).
51. Yasaka, M., Terazawa, K., Kayama, H. & Kon, H. Masting behavior of *Fagus crenata* in northern Japan: spatial synchrony and pre-dispersal seed predation. *Forest Ecology and Management* **184**, 277–284 (2003).
52. Silvertown, J. The evolutionary ecology of mast seeding in trees. *Biological Journal of the Linnean Society* **14**, 235–250 (1980).

Acknowledgements

Author contributions

K.S. and Y.H. conceived the research. K.S. conducted the numerical simulations, the analysis of the results and wrote the manuscript. Y.H. designed the field survey and conducted measurements with A.S.F. and A.I. A.P. and Y.H. participated in discussions and provided valuable suggestions.

Competing interests

The authors declare no competing interests.

Additional information

Supplementary information is available for this paper at https://doi.org/10.1038/s41598-019-50815-8.

Correspondence and requests for materials should be addressed to K.S.

Reprints and permissions information is available at www.nature.com/reprints.

Publisher's note Springer Nature remains neutral with regard to jurisdictional claims in published maps and institutional affiliations.